JGR Oceans

RESEARCH ARTICLE
10.1029/2018JC014581

Special Section:
Forum for Arctic Modeling and Observational Synthesis (FAMOS) 2: Beaufort Gyre phenomenon

Advancing Short-Term Forecasts of Ice Conditions in the Beaufort Sea

M. Yaremchuk[1], T. Townsend[1], G. Panteleev[1], D. Hebert[1], and R. Allard[1]

[1]Naval Research Laboratory at Stennis Space Center, Hancock County, MS, USA

Abstract Numerical experiments with a regional configuration of the CICE model (Los-Alamos Community sea Ice CodE) in the Beaufort Sea assimilating Special Sensor Microwave Imager/Sounder ice concentration (IC) and CryoSat ice thickness (IT) data acquired for September–December of 2015 are presented. We explore sensitivity of the 24-hr IT/IC forecast skill to the system updates, which include introduction of the IT assimilation capability, flow-dependent correlations, and Gaussianization of IC innovations. Experiments with IC data assimilation have shown that the flow-dependent correlations provide 5–7% improvement of the forecast skill during the freezing period (10 September to 10 November) while Gaussianization contributes an additional improvement of 3–4% in most of the cases. In winter (11 November to 31 December) IC assimilation did not produce any statistically significant improvement of the skill due to the loss of dynamical information in the IC fields associated saturation of the ice cover. In contrast, IT assimilation provides larger improvement in December compared to October–November due to the better coverage of the Beaufort Sea by observations and their higher relative accuracy in winter. Comparison of the IT forecast fields with independent in situ observations by two upward looking sonars demonstrates statistically insignificant improvements. Much better improvement (15–25%) is observed when comparing monthly mean IT assimilation runs against independent Advanced Microwave Scanning Radiometer for Earth observing system (AMSR-E) data. Introduction of the heuristic in situ IC/IT correlations into the background covariance model did not produce any improvements of the forecast skill.

Plain Language Summary Four-month-long observations of ice concentration and thickness in the Beaufort Sea are processed using an updated version of the Navy Coastal Ocean Data Assimilation system run at 2-km resolution. The updates include introduction of the ice thickness assimilation capability, flow-dependent correlations, and improvement of the error statistics for ice concentration. We show that daily forecasts of ice conditions improve considerably during the freezing period in September–November. Causes of the improvement are discussed in the context of ice information content of the satellite data.

Key Points:
- Ice concentration and thickness data collected in the Beaufort Sea in September–December 2015 were assimilated into a numerical model
- The 24-hr forecast skill of the model was improved
- Improvement is achieved by introducing ice thickness assimilation capabilty, flow-dependent correlations, and Gaussianization

Correspondence to:
M. Yaremchuk,
max.yaremchuk@nrlssc.navy.mil

Citation:
Yaremchuk, M., Townsend, T., Panteleev, G., Hebert, D., & Allard, R. (2019). Advancing short-term forecasts of ice conditions in the Beaufort Sea. *Journal of Geophysical Research: Oceans*, *124*, 807–820. https://doi.org/10.1029/2018JC014581

Received 25 SEP 2018
Accepted 3 JAN 2019
Accepted article online 14 JAN 2019
Published online 1 FEB 2019

1. Introduction

Recent studies demonstrate a substantial declining trend in area and volume of the Arctic ice cover at the average rates of 10^5 km^2 and 600 km^3 per year (e.g., Cavalleri & Parkinson, 2012; Kwok et al., 2009; Serreze & Stroeve, 2015). This decline means a significant expansion of navigable areas in the near future, which in turn requires more timely and improved forecasting of the ice conditions in the Arctic that was reflected in a rapid progress of ice data assimilation (DA) during the last decades.

Ice concentration (IC) remains a key parameter in the ice DA due to its importance in the ice model dynamics and the abundance of the respective data from satellites. IC assimilation techniques are usually similar to the ones developed for other ocean state variables and range from nudging (Lindsay & Zhang, 2006; Tietsche et al., 2013) and optimal interpolation (Stark et al., 2008; Wang et al., 2013) to ensemble Kalman filtering (Lisäter et al., 2003; Shlyaeva et al., 2016; Yang et al., 2015) and variational methods (Fenty & Heimbach, 2013; Koldunov et al., 2013, 2017).

Ice thickness (IT), an equally important parameter for Arctic navigation, has rarely been used in DA because of sparse in situ data and relatively high observational errors of the space-borne platforms such as CryoSat (Ricker et al., 2014) and Soil Moisture and Ocean Salinity (SMOS) mission (Tian-Kunze et al., 2014). Lisäter et al. (2007) was one of the first to demonstrate the importance of assimilating CryoSat IT data on the performance of a coupled ice-ocean model. More recently, Yang et al. (2014, 2016) investigated assimilation of SMOS IT data into a coupled sea-ice model using a localized Kalman filter and demonstrated a

significant improvement of IT forecasts in the regions of the first-year ice. In their latest study, Mu et al. (2018) assimilated combined SMOS and CryoSat-2 data jointly to extend the improvement of the model's performance into the perennial ice.

The vast majority of the above-mentioned studies focus on the improvement of model predictions on spatial scales significantly larger than 20 km. The objective of the present study is to explore the ways to improve the Navy short-term (24-hr) IC/IT forecasts at 2-km spatial resolution by upgrading the Navy Coupled Ocean Data Assimilation (NCODA) system (Cummings, 2005; Cummings & Smedstad, 2013) with new features. These features include IT assimilation capability, introduction of flow-dependent correlations coupled with nonlocal observations, and Gaussianization of IC innovations. The latter feature is introduced to account for non-Gaussianity of the IC/IT error statistics in the NCODA environment, which is based on Gaussian assumptions. In contrast, the ice error distributions strongly depend on the observed values of the respective fields when they are close to the natural bounds of variation and, therefore, require special treatment (e.g., Barth et al., 2015; Bertino et al., 2003; Bocquet et al., 2010). We also address the issue of the forecast skill sensitivity to variations in formulation of the background error covariance and observation operators. In a separate series of assimilation runs, we explore the impact of IT observations on the system's performance. The related DA experiments were performed with the Los Alamos Community Ice CodE (CICE; Hunke et al., 2015) running in the Beaufort Sea at 2-km resolution.

The paper is organized as follows. The next section contains a description of the experimental setting and the basic features of the Global Ocean Forecast System (GOFS 3.1, Metzger et al., 2015) used for initialization and forcing of the 2dVar CICE DA runs. In section 3, we present the results of the DA runs and assess the efficiency of the NCODA updates in terms of the forecast skill improvement and consistency with independent observations. Summary and discussion of the results conclude the paper.

2. Methodology

2.1. The Assimilation System

The 2dVar DA experiments were performed with CICE forced by atmospheric fields from the Navy Global Environmental Model (NAVGEM 1.2, Hogan et al., 2014) and oceanic fields from the operational run of the GOFS 3.1 DA system. The DA component of GOFS 3.1 (NCODA) sequentially updates the HYCOM-CICE states using the variational DA technique (Cummings & Smedstad, 2013) with two-way coupling between the HYCOM and CICE. The NCODA update $\delta\mathbf{x}$ of the forecast IC/IT fields is given by the relationships

$$\delta\mathbf{x} = \mathbf{VCH}^{\mathrm{T}}\left(\mathbf{HCH}^{\mathrm{T}} + \mathbf{I}\right)^{-1}\delta\mathbf{y}, \tag{1}$$

$$\mathbf{H} = \mathbf{R}^{-1}\widetilde{\mathbf{H}}\mathbf{V}; \qquad \delta\mathbf{y} = \mathbf{R}^{-1}\delta\widetilde{\mathbf{y}}, \tag{2}$$

where $\mathbf{C}$ is the forecast error correlation matrix whose elements depend only on the distance between the correlated points, $\mathbf{V}$ and $\mathbf{R}$ are the respective forecast and observation root mean square error variance matrices, $\mathbf{I}$ is the identity matrix, $\widetilde{\mathbf{H}}$ is the matrix representation of the linear operator interpolating state variables from the model grid on the respective observation locations, and $\delta\widetilde{\mathbf{y}}$ is the vector of the model-data misfits at the observation points.

Daily oceanic and 3-hourly atmospheric fields from the NAVGEM and GOFS 3.1 operational runs between 10 September 2015 and 31 December 2015 were interpolated onto the 512×592 curvilinear orthogonal grid (Figure 1) with 2-km horizontal resolution and then used to force the respective fine resolution CICE model run. Excluding land, the 2-D model domain had $N = 237{,}773$ grid points. The forcing fields were the upper layer ocean velocity, sea surface temperature, sea surface salinity, atmospheric wind stress, air temperature, specific humidity, and shortwave and longwave radiation fields at the surface. At the open boundaries of the domain CICE fields were relaxed to those of the GOFS reference run in a 40-km-wide sponge layer in which relaxation times varied linearly between 0.16 and 24 hr at the outermost and innermost boundaries.

The CICE run was sequentially updated with 2dVar IC/IT increments $\delta\mathbf{x}$ computed either with the standard, that is, operational, or updated formulations of NCODA. In both formulations, the analysis equation (1) involves only IC/IT fields and remains unchanged, but in the updated formulations the correlation matrix $\mathbf{C}$ is specified as an operator in state space, and Gaussianization was applied to the IC innovations

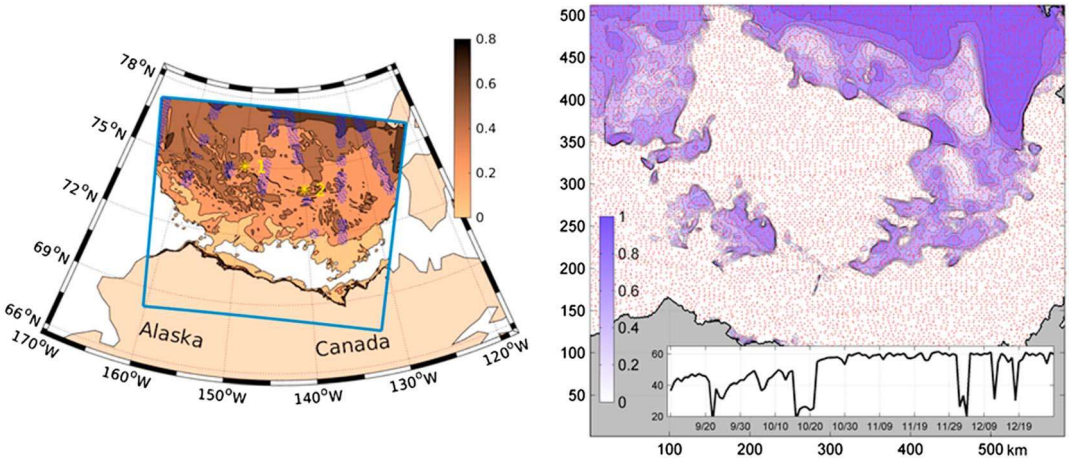

Figure 1. Left: Experimental domain with the Community Ice Code model ice thickness (meters) at the start of ice thickness assimilation on 21 October with CryoSat-2 observations shown in blue. Yellow asterisks indicate locations of the bottom-tethered moorings A (labeled 1) and D (2) deployed in the framework of Beaufort Gyre Observing System study (Proshutinsky et al., 2009). Right: Community Ice Code ice concentration forecast on 17 September 2015. Red dots show combined daily observations of ice concentration by Special Sensor Microwave Imager/Sounder and Advanced Microwave Scanning Radiometer platforms. Time variation of the total number of observations (in thousands) is shown in the insert.

(section 2.3). After NCODA provided IC/IT increments, the CICE initial conditions for IC and ice volume (a product of IT by the grid cell ice area) in different categories were updated in two stages. First, IC increment was sequentially distributed among the ice categories starting from the thinnest one and constrained by the condition that the ice volume update in each category did not produce IT values beyond the boundaries for that category. We used five ice categories with lower boundary values of 0, 0.64, 1.39, 2.47, and 4.57 m (Hunke et al., 2015). After that, the IT increment was used to calculate the net ice volume update, and the latter was used to distribute ice volume updates among the categories in the similar manner.

2.2. Data

2.2.1. Ice Concentration

The IC observations used in this study were derived from the Special Sensor Microwave Imager/Sounder (SSMIS) and Advanced Microwave Scanning Radiometer (AMSR2) sensors. These instruments have footprints of 70×45 and 24×16 km at, respectively, 25- and 10-km resolution. With approximately 14 orbits per day, the satellites provide daily coverage of the experimental domain at approximately 5- to 7-km resolution (right panel in Figure 1). In addition, we used the Interactive Multisensor Snow and Ice Mapping System product (Helfrich et al., 2007) to correct IC errors of the passive microwave sensors emerging at the ice edge in September–October.

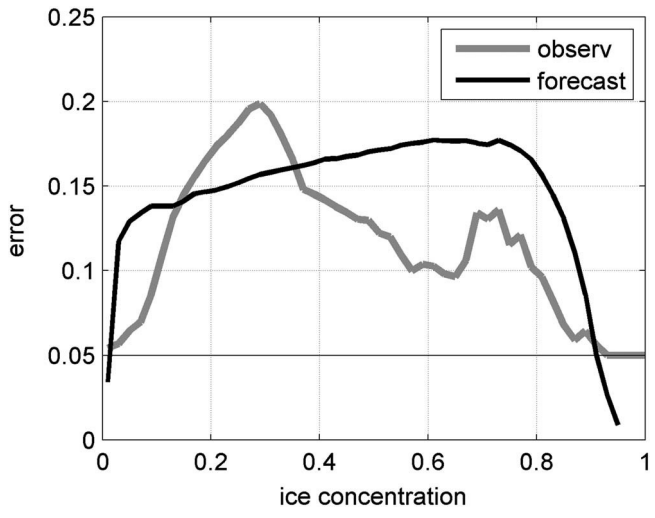

Figure 2. Dependence of the observation and forecast ice concentration root mean square error variances on the background ice concentration values retrieved from the operational Navy Coupled Ocean Data Assimilation run averaged over the assimilation domain between 10 September 2015 and 13 November 2015.

Observations entering the vector $\delta\tilde{\mathbf{y}}$ were SSMIS and AMSR2 ICs acquired within the 24-hr window centered on 12Z analysis time. As a result, the computational domain received daily coverage of $2–5 \times 10^4$ observations (inset in the right panel of Figure 1). On the average, there was one observation per five grid points in the domain, and the observation operator $\mathbf{H}$ had a 4×4 interpolation stencil; that is, interpolation was performed using model values in 16 grid points surrounding an observation. NCODA uses the diagonal RMS observation error variance matrix $\mathbf{R}$ with the minimum RMS error σ of 0.05 (gray line in Figure 2). In the numerical experiments described below, observations with IC values less than 0.1% were assumed to be open water and prescribed to have the minimum value of σ. At the daily analysis times (12Z) the NCODA also provides an estimate of the forecast root mean square error $\mathbf{v} = \mathrm{diag}\,\mathbf{V}$ (black line in Figure 2) based on the previous history of assimilation with the time-

weighting function applied to the respective increment fields. In the open water the diagonal elements of **V** were bounded from below by 0.001.

2.2.2. Ice Thickness

The source of IT data was the 2-day-averaged CryoSat-2 observations from the Center for Polar Observations and Modeling (http://www.cpom.ucl.ac.uk/csopr/seaice.html). These observations have a relatively small footprint (0.3 × 1.6 km), which allows to measure sea ice freeboard and estimate IT using a combination of the freeboard measurements and estimates of snow depth and density derived from a climatology (Warren et al., 1999). CryoSat-2 satellite tracks (Figure 1, left panel) cover the Arcic basin up to 88°N and provide statistically confident IT estimates in the areas of relatively high (>0.5 m) IT. Laxon et al. (2013) conducted a detailed description of the CryoSat-2 data processing, and a brief analysis of the possible errors in the IT observations. The errors are mostly due to uncertainties in estimation of the snow loading and ice/water densities, employed when converting freeboard to IT. More recently, King et al. (2018) utilized the in situ IT observations in the area north of Svalbard and found that in this region covered by deep (~1 m) snow, CryoSat-2 tends to overestimate IT by 50–100%. Taking into account that snow loading should be less significant at the beginning of the winter season, we use data from http://www.cpom.ucl.ac.uk/csopr/seaice.html portal with minor averaging over the surrounding (located within 4 km from a data point) model bins and without any bias correction.

Compared to IC data, IT observations were approximately 10 times less numerous, and, therefore, their assimilation required additional validation. For that purpose, we used two independent data sets. The first one contains in situ ice draft observations obtained from two bottom-tethered moorings deployed in the framework of Beaufort Gyre Observing System study (Proshutinsky et al., 2009). The Upward Looking Sonars positioned 50 m below the surface recorded the ice draft. Daily averaged observations were converted into IT using the algorithm of Bourke and Paquette (1989) with the regression ratio of 1.115. For larger-scale validation of the IT assimilation, we also used monthly mean estimates of ice draft in the November and December from AMSR-E radiometer converted into IT using the algorithm of Tateyama et al. (2013). The method was adjusted to the Beaufort Sea region using calibration against the mooring data described above (see Krishfield et al., 2014, for a detailed description of the data conversion).

2.3. Updates of the Assimilation Algorithm

For this study, we modified NCODA's assimilation in several aspects and investigated sensitivity of the forecast skill to these changes. The major modifications considered are introduction of the (a) nonlocal footprints of satellite observations, (b) flow-dependent correlations, (c) IT assimilation capability, and (d) Gaussianization of the IC innovation statistics.

2.3.1. Nonlocal Observation Operators

The numerical implementation of equation (1) in NCODA is tailored for accurate treatment of pointwise observations using analytic expressions for the matrix elements of **C**. In particular, the operator $\widetilde{\mathbf{H}}$ is used in NCODA only for computing the innovations, while the elements of the matrices $\mathbf{CH}^{\mathrm{T}}$and $\mathbf{HCH}^{\mathrm{T}}$ are computed explicitly under the assumption that the respective observations are made exactly at the locations specified by the geographical coordinates of the data points. In reality, IC/IT observations from satellites have finite footprints whose size is several times larger than the model grid step (see section 2.2). Therefore, it could be more practical to consider the finite footprint size and explicitly use interpolation operators **H** with the observation footprint size in computing the products $\mathbf{CH}^{\mathrm{T}}$ and $\mathbf{HCH}^{\mathrm{T}}$. In the present study, we used 2-D spline interpolation with the footprint size of 8 × 8 km, which is consistent with the resolution of both IC and IT satellite data sets.

2.3.2. Flow-Dependent Correlations

Nonlocal treatment of observations requires specifying the correlation matrix **C** on the model grid. A numerically efficient method of doing this is to represent the action of **C** on a state vector by a rational function of the diffusion operator. This technique has been used in oceanographic practice for several decades in isotropic/homogeneous settings (e.g., Derber & Rosati, 1989; Di Lorenzo et al., 2007; Egbert et al., 1994; Weaver & Courtier, 2001; Weaver et al., 2003). More recently, it was adopted for inhomogeneous case (e.g., Beckers et al., 2014; Weaver & Mirouze, 2013; Weaver et al., 2015; Yaremchuk & Carrier, 2012; Yaremchuk et al., 2013), but its applications in operational oceanography are rare. In the present study,

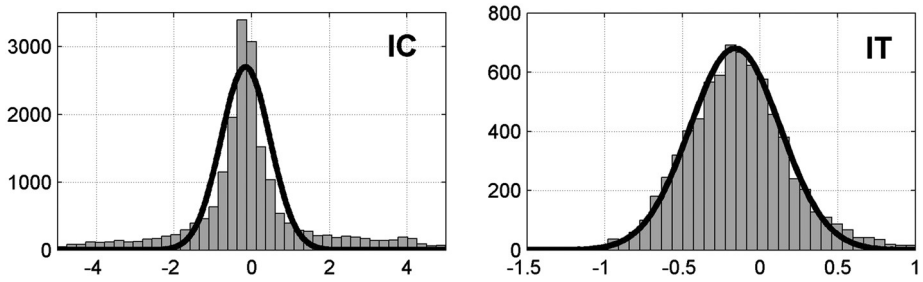

Figure 3. Left: the histogram of ice concentration (IC) innovations on 25 September 2015 obtained from the standard Navy Coupled Ocean Data Assimilation run in the model domain by excluding the open water points. Right: ice thickness (IT) innovations on 20 December 2015. Innovations are normalized by the respective observation errors. Vertical axes show the number of values within a bin. The best fit to the histograms by the Gaussian curve (black line) is shown to illustrate the departure of the innovation statistics from Gaussianity.

we implement the action of **C** on a state vector by explicit solution of the diffusion equation with anisotropic and horizontally inhomogeneous diffusion tensor, whose principal axes orientation and magnitude are defined by the background ice velocity field (Yaremchuk & Nechaev, 2013). In addition, we explored the impact on the forecast skill of a heuristic model characterizing local IC/IT correlations. More details on the adopted correlation model can be found in the appendix.

2.3.3. Gaussianization

Error statistics of temperature, salinity, velocity, and sea surface height fields can be described by the Gaussian probability density function (pdf) within a reasonable degree of accuracy because the magnitude of respective fluctuations is too small for the pdfs to be affected by the natural bounds of variability of these quantities. In contrast, IC and IT are strictly bounded from below by zero, while IC has an additional constraint IC < 1. These constraints considerably affect the daily error statistics, especially when the ice fields approach open water condition (zero value) or, in the case of IC, to complete ice cover.

Preliminary analysis of the innovation statistics has shown that IT errors could be approximated by the Gaussian pdf with a reasonable degree of accuracy (right panel in Figure 3), while IC errors were characterized by a much larger departure from Gaussinaity (Figure 3, left panel). This could be explained by the fact that CryoSat-2 observations are predominantly acquired in regions of relatively thick ice, where IT values are rather far from zero, where the typical observation errors range within 20–40% of the observed values. On the contrary, the normalized SSMIS observations have many points with low concentrations, which predominantly populate the sharp central peak in the left histogram of Figure 3. The long tails can be attributed to the errors in the position of thick ice field edges whose IC values are close to 1, while the NCODA-generated observation errors can sometimes be as low as 0.2–0.3.

This analysis reveals a certain inconsistency between the update formula (1) derived under the Gaussianity assumption and the IC error statistics exposed in Figure 3. In an attempt to remove this disagreement, the normalized IC innovations were transformed prior to the daily analyses by applying the standard Gaussianization technique (e.g., Brankart et al., 2012). The simplifying assumptions were independence of the transformation function on horizontal coordinates and validity of the NCODA background correlation matrix **C** (equation (1)) in Gaussianized variables. After the solving equation (1), the inverse of the Gaussianization transform was applied to the IC increments before the standard NCODA postprocessing was made to obtain the final analysis. Although the utilized approach does not impose strong constraint on the limits IC variation, it still provides a more consistent treatment of the IC innovation statistics, especially in the tails clearly visible in the left panel of Figure 3.

2.3.4. IT Assimilation

IT data were treated similar to IC with the only exception that Gaussianization was not performed prior to the analysis. The IT correlation matrix was identical to the matrix **C** used for IC assimilation (see the appendix).

To explore the impact of IC-IT cross-correlations on the forecast skill, we assumed the following form of the joint correlation matrix:

$$\mathbf{C}_{ct} = \begin{bmatrix} \sqrt{\mathbf{C}} & \mathbf{0} \\ \mathbf{0} & \sqrt{\mathbf{C}} \end{bmatrix} \begin{bmatrix} \mathbf{I} & \mathbf{D}_{ct} \\ \mathbf{D}_{ct} & \mathbf{I} \end{bmatrix} \begin{bmatrix} \sqrt{\mathbf{C}} & \mathbf{0} \\ \mathbf{0} & \sqrt{\mathbf{C}} \end{bmatrix}, \tag{3}$$

where $\mathbf{D}_{ct}$ is the diagonal matrix whose nonzero elements $D_{ct}(\boldsymbol{x})$ are defined by the local IC values $c(\boldsymbol{x})$ as follows:

$$D_{ct}(\boldsymbol{x}) = \gamma\left\{1-4[c(\boldsymbol{x})-0.5]^2\right\}. \tag{4}$$

With this formulation IC-IT correlations are positive, reach the maximum value (defined by the tunable parameter $0 < \gamma < 1$) at $c = 0.5$, and vanish at the boundaries of IC variation. The factorized representation (3) keeps the spatial structure of cross-correlations similar to the adopted correlation model and maintains the positive-definite property of $\mathbf{C}_{ct}$.

3. Results

In this section we explore sensitivity of the NCODA performance with respect to the modifications of the assimilation procedure described in section 2. Performance of the system was evaluated in terms of the 24-hr forecast skill S, computed using the methodology of Hebert et al. (2015), who assessed skill improvement of the Arctic Cap Nowcast Forecast System (ACNFS) using the following formula:

$$S^n(a|r) = 1-\frac{\left(\widetilde{\mathbf{H}}\mathbf{x}_a^n-\widetilde{\mathbf{y}}^n\right)^T\left(\widetilde{\mathbf{H}}\mathbf{x}_a^n-\widetilde{\mathbf{y}}^n\right)}{\left(\widetilde{\mathbf{H}}\mathbf{x}_r^n-\widetilde{\mathbf{y}}^n\right)^T\left(\widetilde{\mathbf{H}}\mathbf{x}_r^n-\widetilde{\mathbf{y}}^n\right)}, \tag{5}$$

where $\mathbf{x}^n{}_a$ and $\mathbf{x}^n{}_r$ are the analyzed and reference 24-hr forecasts at nth time and $\widetilde{\mathbf{y}}^n$ is the respective vector of IC observations. In the following, we will use two types of reference forecasts. The first type is computed using the assumption of IC/IT persistence during the 24-hr period (Hebert et al., 2015) and abbreviated by p. The second type, denoted by s, is taken from the standard (nonmodified) NCODA (NC) run. Using this notation, the forecast skill of a run featuring a modification m with respect to the standard NC run is denoted by $S(m|s)$ among others. Statistical significance of the time-averaged forecast skill was assessed by comparison with the standard deviation obtained by averaging over the respective time interval.

3.1. Flow-Dependent Correlations and Nonlocal Observations

Experiments with the flow-dependent IC correlation model (hereinafter abbreviated by f) were conducted with drift velocities $\boldsymbol{u}$ taken from the background CICE fields used in the analyses. During the assimilation period (10 September 2015 to 31 December 2015), 90% of CICE ice velocities did not exceed 0.3 m/s, with only 0.25% of the velocities being larger than 0.6 m/s, and sometimes reaching 1–1.3 m/s in magnitude. The horizontal variation of $\boldsymbol{u}$ had a typical scale of 100–200 km, indicating that ice was primarily driven by winds.

The IC forecast skill (equation (4)) computed with respect to the assimilation run with the homogeneous correlation model shows the flow-dependent correlations provide certain improvement of the skill (positive values in Figure 4, right axis). The improvement is statistically significant in September (0.07 ± 0.03) and to a lesser extent (0.05 ± 0.04) in October. During these months, a considerable part of the Beaufort Sea was ice-free, and changes in ice cover better reflected the impact of drift due to higher spatial variations of the IC values. Starting from 25 October, more than 90% of the sea was covered by ice (blue line in Figure 4), and the area-mean IC values quickly rose above 90% by the beginning of November, whereas their RMS variation dropped from 35% in October to 3% in November. Consequently, the IC field lost information on ice motion causing gradual reduction of S by the flow-dependent correlation model to a statistically insignificant ($-0.8 \pm 1.9\%$) value in November–December. It is noteworthy that winter freezing had similar diminishing effect on the forecast skill in the experiments with Gaussianization (section 3.3).

Model runs with assimilation using nonlocal observation operators (abbreviated by n) did not produce any statistically significant improvement of the skill for both flow-dependent and isotropic correlation models. The respective values of $S(n|s)$ averaged over the "open water period" (10 September 2015 to 13 November 2015 in Figure 4) were found to be $-0.6 \pm 3.7\%$ and $0.2 \pm 2.3\%$, respectively. We partly attribute the result

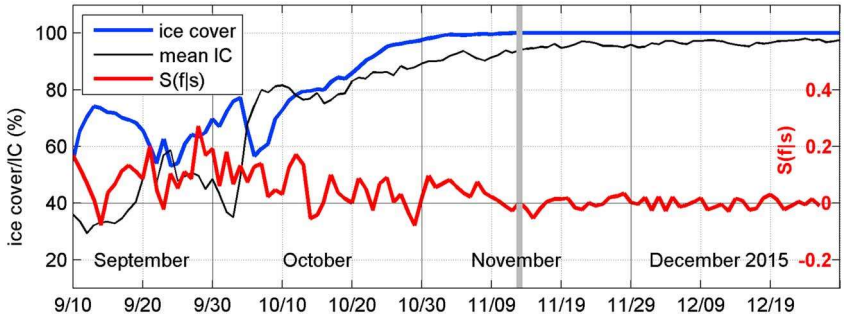

Figure 4. Percent of the domain in Figure 1 occupied by ice-covered areas (blue line) and the mean ice concentration (IC) averaged over these areas (thin black line). The red line (labeled on the right axis) shows $S(f|s)$ values over the entire time interval. The vertical gray line delineates the end of the "open water period" (10/9–13/11.2015), when IC variations were strong enough to contain information on ice dynamics.

to a relatively small (5–7 km) footprint of SSMIS observations compared to model grid step, so that the effect of taking the correct spatial interpolation stencil was lost on the background of much larger errors associated with uncertainties in the correlation model and error statistics generated by NCODA.

3.2. Impact of Gaussianization

Similar to experiments with flow-dependent covariances, experiments with Gaussianization (hereinafter abbreviated by g) demonstrated noticeable improvement of the skill only during the open water period (10 September to 13 November).

Figure 5 shows the time dependence of $S(g|s)$, $S(g|p)$, and $S(s|p)$ during this period. The value of $S(g|s)$ (thick blue line in Figure 5) stays positive most of the time with the average value of 0.09, which appears to be quite substantial compared to $S(s|p) = 0.40$ reported by Hebert et al. (2015) for the ACNFS in February–June 2015. It is noticeable that time dependence of $S(g|s)$ is characterized by two distinct periods. The first month (10 September 2015 to 9 October 2015) has a moderate skill improvement ranging within 0.03–0.07 and several instances of slightly negative skill. This period was characterized by a relatively stable ice-covered area (55–65%, thick blue line in Figure 4) with the mean IC gradually increasing from 35% to 70%. In the next period (9 October 2015 to 13 November 2015), the computational domain was subject to rapid freezing and became completely ice covered by 15 November (the mean IC increased from 70% to 96%). During this rapid transition period, the impact Gaussianization was more profound, with the values of $S(g|s)$ averaging to 0.17. As noticed earlier, starting from mid-November, the values of $S(g|s)$ dropped dramatically, demonstrating no improvement with respect to the standard NCODA run.

Comparison between the Gaussianized and standard NCODA runs made with respect to persistence (thin black and blue lines in Figure 5, respectively) also shows a noticeable impact: the time-averaged value 0.37 of $S(g|p)$ is almost 20% better than $S(s|p)$. It should be noted that compared to the pan-Arctic run of Hebert et al. (2015), our experiments were conducted at two times higher (2 km vs. 3.5–4 km) spatial

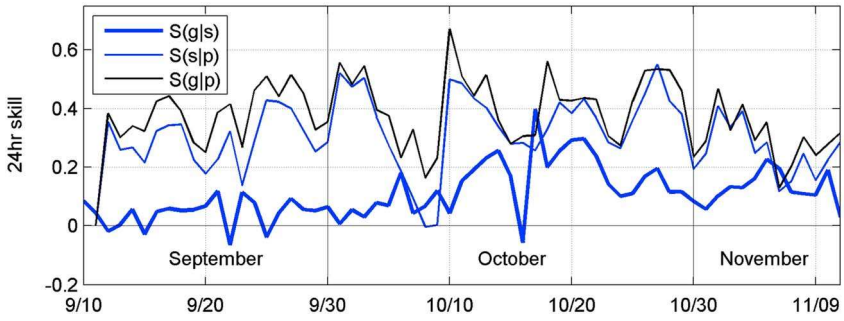

Figure 5. The forecast skill of the NC (thin blue line) and gNC (thin black line) runs with respect to persistence. Thick blue line shows the gNC skill with respect to NC run.

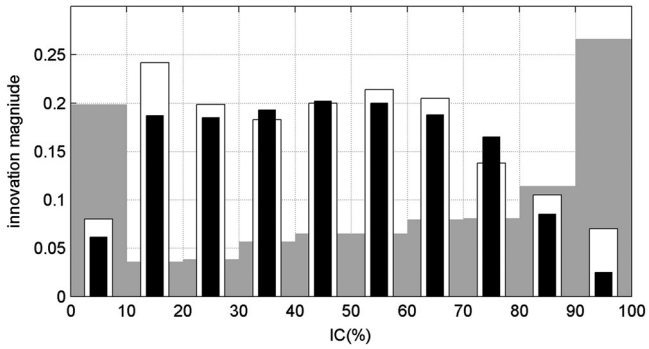

Figure 6. Distribution of the space and time-averaged innovation magnitudes over 10 ice concentration (IC) categories for the NC run (white bars) and gNC run (black bars). Gray bars show relative numbers of the respective observation points.

resolution in a smaller domain, resulting in a relatively small value of $S(s|p) = 0.31$ (thin blue line in the Figure 5) and a relatively high (up to 20%) improvement of the forecast skill.

Statistics of the increments produced by the NC and gNC assimilation runs (Figure 6) demonstrate that Gaussianization tends to be more beneficial at locations with IC close to its range boundaries (0 and 1), where the Gaussianity assumption underlying the analysis equation (1) becomes invalid. It is noteworthy that the respective innovations occur more often in the vicinity of the abrupt changes in IC near the ice edge when either open water or a high IC value are observed against the opposite background. In other words, IC innovations near the ice edge have a tendency to populate the tails of the $\delta\mathbf{y}$ histogram in Figure 3. In the standard NCODA run these extreme innovations generate persistently larger increments compared to the Gaussianized case and, therefore, have a tendency to produce larger and more frequent shocks to the model state than it was assumed in the derivation of the analysis equation (1). In that respect, a more consistent treatment of the innovation statistics at the ice edge provides the major contribution to the improvement of the forecast skill by the Gaussianized run.

3.3. IT Assimilation

A series of numerical experiments were conducted to assess the impact of IC-IT cross-correlations on the performance of NCODA. Since the heuristic model (equations (3)–(4)) is far from perfection, we varied the maximum correlation parameter $\boldsymbol{\gamma}$ in an attempt to detect improvements in the forecast skill. Experiments were conducted in the flow-dependent mode of $\mathbf{C}$ without IC Gaussianization but failed to provide a statistically significant improvement of the forecast skill compared to the case with zero IC-IT cross-correlations ($\mathbf{D}_{ct} = 0$ in equation (3)).

We attribute this failure to the "complimentary" nature of SSMI and CryoSat-2 observations in terms of the forecast skill improvement: As noted in the previous section, IC assimilation delivers a statistically significant improvement only in September–October (Figure 4), while in November–December IC fields are too close to saturation (100%) and contain no useful information on ice dynamics. On the contrary, CryoSat-2 observations are completely absent before October 21, being most abundant and accurate in November–December, when IC data become practically useless in terms of supplying additional information on the CICE state. In that respect, augmenting CryoSat-2 data with SMOS observations that cover regions with intermediate IC values (Mu et al., 2018) may potentially result in noticeable IC-IT coupling of error statistics and therefore have better potential for the forecast skill improvement.

Figure 7 highlights the major results of the combined IC/IT assimilation. The most prominent impact is a significant (~20 cm or ~20–25%) decrease of the domain-averaged IT in the run with assimilation (dashed

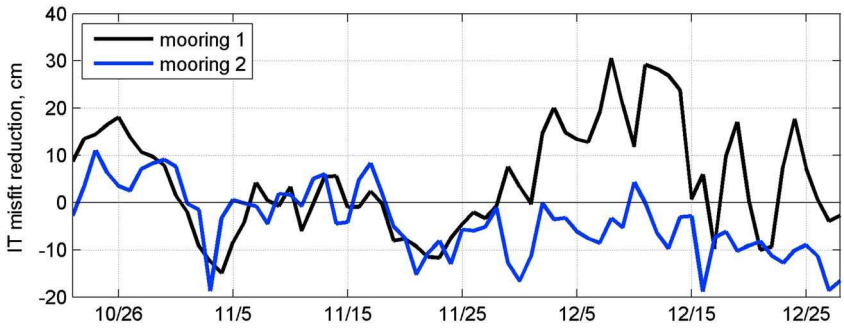

Figure 7. Domain-averaged absolute value of the model-data misfits (cm) between the 24-hr forecasts produced by the runs with (thin solid line) and without (thin solid line) assimilation of CryoSat-2 data. Black segments on the thick solid line indicate periods of ice thickness (IT) forecast improvement by assimilation. The blue dashed line shows decrease of the domain-averaged IT caused by IT assimilation.

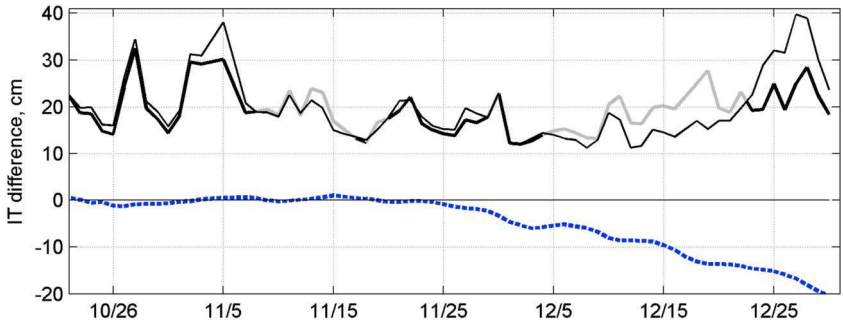

Figure 8. Reduction of the model-data misfits in two moorings produced by assimilating CryoSat-2 ice thickness (IT) data. Positive values correspond to smaller misfits of the assimilation runs.

line in Figure 7). This agrees well with the results of the Allard et al. (2018), who found that ACNFS system tends to overestimate the mean IT without proper initialization using CryoSat-2 observations. It is interesting that the effect of the CryoSat-2 DA is negligible in period of rapid ice cover expansion (late October–November) until the mean IT over the domain reaches 0.5–0.6 m by 25 November. After that, the model without assimilation has a visible tendency to overestimate the ice accumulation in the area. This is clearly seen from the linear trend of approximately 0.5 cm/day visible during 11/25–12/31 (dashed line in Figure 7). The effect could be attributed to the fact that CryoSat-2 data in November are mostly available only for the northern part of the region, where IT exceeds 0.5 m. The southern part of the domain is ice-free or covered by the thin ice barely detectable by the observations. Therefore, the integrated impact of assimilating the CryoSat-2 data should be less visible before the 25 November. After that, the entire Beaufort Sea basin was covered by relatively thick (well-observed) ice resulting in less ice production in December by the assimilation run.

Solid lines in Figure 7 demonstrate model-data misfits computed for 24-hr forecast fields with and without IT assimilation. Although IT assimilation demonstrates a certain improvement (decrease) of the forecasted misfits (70% of time, and 0.4 ± 3.8 cm in the time average), it appears to be statistically insignificant. This can be explained by sparse daily coverage of the domain by the CryoSat-2 tracks: Consecutive tracks cross the model domain in a random pattern (a typical example shown in Figure 1). As a consequence, the mean distance (~110 km) between observation points separated by 24 hr in time is considerably larger the typical displacement (10 km) of the IT field features in the same period.

A more reliable validation of the assimilation quality can be obtained by comparison with independent IT observations. Figure 8 shows improvement in IT model-data misfits derived from the in situ ice draft data on two moorings (yellow stars in the left panel of Figure 1) deployed in the Beaufort Sea during the assimilation period (section 2.2.2). The model-data misfits at the first mooring demonstrate a statistically significant (4.8 ± 4.6 cm) improvement during the observation period, while the results from the second mooring appear to be less conclusive (-3.9 ± 4.1 cm). Note that improvement on the first mooring is especially significant in December, when ice cover was considerably thicker and the CryoSat-2 data were available at the mooring locations two times more often than in October. The second mooring location was less covered by CryoSat-2 observations (four track crossings vs. six for the first mooring) and had much larger discrepancy with in situ data compared to the first mooring (0.4 m vs. 0.2 m). This may partly explain worse skill of IT assimilation versus in situ data at the second mooring, which may also be attributed to a somewhat larger bias estimate at that location. However, due to a small number of CryoSat-2 crossings of the mooring locations, it is difficult make more confident conclusions due to large errors in bias estimates.

Monthly averaged AMSR-E IT data described in section 2.2.2 allow obtaining a more statistically reliable validation, partly because IT estimates derived from AMSR-E by Krishfield et al. (2014) were carefully calibrated against numerous ice draft observations from all available moorings deployed in the Beaufort Sea during the period and, therefore, could be considered to be unbiased. We found that assimilation of IT data from CryoSat-2 results in 15% to 25% reduction of the monthly and spatially averaged model-data difference in November and December, respectively. We assume that this improvement is statistically significant compared to the above assessment via in situ data at two locations. The improvement also indicates that AMSR-

E/CryoSat-2 bias during this period was considerably smaller than the bias between nonassimilative model runs and CryoSat-2 data.

3.4. Combined Effects

Additional experiments were performed to assess NCODA's performance with different combinations of the updates outlined in section 2. As expected, the largest effect was achieved by combining the flow-dependent correlations ($S(f|s) = 6.7\%$) with Gaussianization, which produced the overall $S(fg|s) = 9.9\%$ improvement in the forecast skill. Robustness of the effect was additionally tested against the standard NCODA run with the second-order autoregressive (SOAR) correlation model (abbreviated by s'). Since the SOAR model cannot be represented by the diffusion equation, the decorrelation scale was adjusted to provide the best approximation of the SOAR function by the Gaussian with the background decorrelation scale $r = 6(8/\pi)^{1/2}$ ~9.2 km (Yaremchuk & Smith, 2011). Improvement in the SOAR case was approximately twice as small ($S(fg|s') = 4.6\%$) as compared to the run with flow-dependent Gaussian correlations. The difference could be attributed to at least two factors: 20% approximation error of the SOAR correlation function by the Gaussian one and a somewhat larger value ($S(s'|p) = 33\%$) of the standard run skill with the SOAR correlation versus persistence.

Experiments with the combined IC-IT assimilation did not detect any statistically significant improvements in either IC or IT forecast skills when IC (IT) observations were augmented by the complimentary IT (IC) type of data. The effect appeared to be robust and insensitive to the variations of the empirical correlation coefficient γ (equation (4)). We attribute this failure to the fact that IC assimilation delivers a statistically significant improvement only in September–October (Figures 4 and 7), while in November–December IC observations become virtually absent due to IC saturation near 100%. On the contrary, IT observations are completely absent until the end of October and become abundant only at the beginning of November when IC data become practically useless in terms of supplying additional information on the CICE state.

It is necessary to note that combined IC-IT did improve the monthly mean misfits with independent AMSR2 observations from 27/43 cm in November/December with IC assimilation only to 24/32 cm in the case when both IC and IT data were analyzed by the system.

4. Conclusions and Discussion

The presented study addresses the issue of improving the short-term (1 day) forecast skill of a high-resolution (2 km) ice model driven by observations collected in the Beaufort Sea during the freezing period (September–December 2015). Improvement of the skill was explored along several lines that are currently not implemented in the operational system: These are the IT assimilation capability, introduction of spatially inhomogeneous flow-dependent correlations coupled with nonlocal observations, and Gaussianization of IC innovations. Performance of system has been tested in a series of 2dVar assimilation experiments with NCODA assimilating SSMIS, AMSR2 IC data, and CryoSat-2 IT observations into the CICE model driven by HYCOM and NAVGEM forcing.

Comparison with NCODA runs performed in the standard (operational) configuration has shown that introduction of the flow-dependent correlations improves the forecast skill by 5–7% during the freezing period (10 September 2015 to 13 November 2015) with no significant impact on the forecast skill later, when the area-mean IC becomes close to saturation. Gaussianization contributes an additional improvement of 3–4% during the freezing period and has no effect on the skill after mid-November.

Introduction of the IT assimilation capability did not show any statistically significant improvement of the 24-hr forecast skill with respect to CryoSat-2 data. We attribute this to the fact that IT features observed on consecutive CryoSat-2 tracks are too far away from each other to be casually related within the 24-hr forecast time frame. The situation may improve in the regions of denser coverage (north of 80°N), where daily CryoSat-2 tracks are separated by less than 50 km and relative accuracy of the observations is higher due to thicker ice. Comparison with independent in situ observations by two upward looking sonars demonstrated only a minor (1–3 cm) improvement at a statistically insignificant level. At the same time, we detected a much more noticeable (15–25% or 3–11 cm) improvement in the model's discrepancy with independent monthly mean AMSR-E IT data (Krishfield et al., 2014). An alternative cross-validation method (e.g., based on withholding a part of CryoSat data) could be performed in the regions with denser

coverage by IT observations, but domain under consideration is covered too sparsely for statistically confident assessment of the 24-hr forecast skill.

Assimilation experiments have also shown that there is no significant improvements in the skill across the two types of ice observations. The result was robust and did not depend on the magnitude of the local IC-IT correlation coefficient γ introduced by the heuristic correlation model (equations (3)–(4)). The IT forecast skill was also insensitive to introduction of the flow dependence in the spatial structure of the correlation model.

The relatively poor results of IT assimilation can be explained by the sparsity of IT data (2×10^5 IT vs. 3×10^6 IC observations) and larger uncertainties of the remotely sensed IT data as compared to IC observations. In particular, a recent study by King et al. (2018) indicates that CryoSat-2 data in the Atlantic sector of the Arctic Ocean could be biased due to the uncertainties in the snow loading estimates. To assess possible impact of this bias, we made three additional assimilation experiments with CryoSat-2 data multiplied by 1.2, 0.8, and 0.6. In all three cases the results were worse than those obtained with original data, suggesting a minor impact of the snow load in the Beaufort Sea. This can be attributed to at least two factors: small snow accumulation in November–December compared to March April and negligible impact of the Atlantic cyclones.

To summarize, our results indicate that introducing flow-dependent covariances and Gaussianization into ice assimilation may improve the short-term forecast skill at fine (2 km) resolution by several percent. However, this conclusion should not be treated as a universal guidance, because improvements may strongly depend on the features of a specific DA system. In particular, flow dependence of the correlation could be better represented by the localized ensemble perturbations than by the heuristic model based on the background drift velocities used in the present study. Availability of the ensemble environment is also essential for consistent transformation of the covariances and for compensating possible biases introduced by the Gaussianization (e.g., Bishop, 2016), especially near the ice edge, or at other locations where the forecast field is close to the limits of its variability.

Due to relatively high uncertainties and sparsity of IT data, and low information content of IC observations in thick ice, the joint IC-IT assimilation failed to reveal statistically significant IC/IT correlations and improvements in the daily IT forecast skill. However, IT observations did have a noticeable positive impact on the assimilation results in terms of the agreement with independent IT observations (in situ moorings, AMSR2 data), especially at large spatial and temporal scales. We believe that much better improvement may take place in the regions to the north of the Beaufort Sea (78–88^{o}N), where the CryoSat-2 data density is significantly higher and the ice cover is more persistent and thicker. At the same time, enriching IT data by SMOS observations may bring new benefits to IC-IT assimilation, because SMOS data extend IT assimilation into the regions with relatively thin ice where IC data are capable to provide more information on ice dynamics.

The major objective of the present study was to improve the forecast skill of the operational (ensemble-free) version of NCODA on relatively short spatial and temporal scales in the absence of the ensemble environment. Because of that, we simplified the standard ensemble-based Gaussianization approach by assuming that the heuristic correlation model was valid in the Gaussianized variables by neglecting horizontal inhomogeneity of the IC statistics. To reduce errors associated with these assumptions, the Gaussianization transform was applied to model-data misfits, preventing the analysis fields to be constrained by the bounds of IC variability and thus requiring additional analysis correction similar to the one present in the operational algorithm running without Gaussianization. Despite these simplifications, the Gaussianization approach resulted in a noticeable improvement of the forecast skill. One may expect more substantial improvement if higher quality observations of ice conditions and/or atmospheric forcing were employed in controlling the models. These advances require substantial expansion of observational networks and improvement remote sensing technology.

Work underway will extend the approach to include SMOS observations into the NCODA. Another prospective line of development is transitioning NCODA to ensemble formulation featuring local Gaussianization transformations of the arbitrary sets of non-Gaussian variables. This activity is planned to start in the near future.

Appendix A: The Background Error Correlation Model

In the present study we employ an implicit representation of the correlation matrix by the kernel of the heat transfer equation, so that the action of **C** on a scalar 2d field $\mathbf{f} = \mathrm{f}(\boldsymbol{x})$ is represented by

$$\mathbf{C}\,\mathbf{f} = \mathbf{N}(\boldsymbol{x})\ \exp\left[1/2\ \ \nabla^{\mathrm{T}}\mathbf{D}(\boldsymbol{x})\ \nabla\right]\mathbf{f}. \tag{A1}$$

Here **N** is the diagonal rescaling matrix of normalization factors, ∇ is the matrix representing the discretized 2-D gradient operator on the model grid, $^{\mathrm{T}}$ denotes transposition, and **D** is the 2-D diffusion tensor field represented by 2×2 positive definite matrices specified in every grid point $\boldsymbol{x}$ of the model domain. The advantage of this formulation is that it guarantees positive definiteness of **C** in strongly inhomogeneous cases (typical for ice dynamics), which may not be handled properly by the current NCODA formulation.

To ensure numerical positive definiteness of the operator in the square brackets of (A1), the diffusion tensor was represented in the square root form $\mathbf{D} = \mathbf{D}^{\mathrm{T}/2}\,\mathbf{D}^{1/2}$ with

$$\mathbf{D}^{1/2}(\boldsymbol{x}) = r\begin{bmatrix}\lambda(\boldsymbol{x}) & 0\\ 0 & 1\end{bmatrix}\begin{bmatrix}\cos\theta(\boldsymbol{x}) & \sin\theta(\boldsymbol{x})\\ -\sin\theta(\boldsymbol{x}) & \cos\theta(\boldsymbol{x})\end{bmatrix},$$

where $r = 6$ km is the isotropic decorrelation scale, λ is the square root of the principal axis of **D**, and θ is its orientation. In the computations, we assumed that the principal axis is aligned with the vector of the ice drift velocity $\boldsymbol{u}$, while $\lambda^2 = \max(1, |\boldsymbol{u}|/u_0)$, where $u_0 = 7$ cm/s is the rms magnitude of isotropic noise defined by the uncertainty of the drift velocity field. As a consequence, the diffusion was isotropic ($\mathbf{D} = r^2\,\mathbf{I}$) in all the grid points where the magnitude of ice drift velocity was less than 7 cm/s.

Acknowledgments
The authors were supported by the Office of Naval Research program elements 0603207N (Navy Earth System Prediction Capability) and 0602435N (Arctic Data Assimilation). All model and quality-controlled observational data used in this study are securely stored at the Navy DSRC archive server and can be accessed after obtaining an account at the facility. The corresponding author can be contacted for information to access the archived data once an account has been established. We are indebted to R. A. Krishfield and A. Proshutinsky who kindly provided monthly mean AMSR-E data and in situ ice draft observations acquired in the framework of the Beaufort Gyre Observing System experiment. Helpful discussions with P. Posey are gratefully acknowledged.

References

Allard, R. A., Sinead, L., Farrell, S. L., Hebert, D. A., Johnston, W. F., Li, L., et al. (2018). Utilizing CryoSat-2 sea ice thickness to initialize a coupled ice-ocean modeling system. *Advances in Space Research*, *62*(6), 1265–1280. https://doi.org/10.1016/j.asr.2017.12.030

Barth, A., Canter, M., Schaeybroeck, B., Vannitsem, S., Massonnet, F., Zunz, V., et al. (2015). Assimilation of sea surface temperature, sea ice concentration and sea ice drift in a model of the Southern Ocean. *Ocean Modelling*, *93*, 22–39.

Beckers, J.-M., Barth, A., Troupin, C., & Alvera-Azcarate, A. (2014). Approximate and efficient methods to assess error fields in spatial gridding with data interpolating variational analysis (DIVA). *The Journal of Atmospheric and Oceanic Technology*, *31*(2), 515–530. https://doi.org/10.1175/JTECH-D-13-00130.1

Bertino, L., Evenesen, G., & Wackernagel, H. (2003). Sequential data assimilation techniques in oceanography. *International Statistical Review*, *71*, 223–241.

Bishop, C. H. (2016). The GIGG-EnKF: Ensemble Kalman filtering for highly skewed non-negative uncertainty distributions. *Quarterly Journal of the Royal Meteorological Society*, *142*(696), 1395–1412. https://doi.org/10.1002/qj.2742

Bocquet, M., Pires, C. A., & Wu, L. (2010). Beyond Gaussian statistical modeling in geophysical data assimilation. *Monthly Weather Review*, *138*(8), 2997–3023. https://doi.org/10.1175/2010MWR3164.1

Bourke, H., & Paquette, R. (1989). Estimating the thickness of sea ice. *Journal of Geophysical Research*, *94*(C1), 919–923. https://doi.org/10.1029/JC094iC01p00919

Brankart, J.-M., Testut, C.-E., Beal, D., Doron, M., Fontana, C., Meinsvielle, M., et al. (2012). Towards an improved description of ocean uncertainties: Effect of local anamorphic transformations on spatial correlations. *Ocean Science*, *8*(2), 121–142. https://doi.org/10.5194/os-8-121-2012

Cavalleri, D. J., & Parkinson, C. L. (2012). Arctic sea ice variability and trends, 1979–2010. *The Cryosphere*, *6*(4), 881–889. https://doi.org/10.5194/tc-6-881-2012

Cummings, J. (2005). Operational multivariate data assimilation. *Quarterly Journal of the Royal Meteorological Society*, *131*(613), 3583–3604. https://doi.org/10.1256/qj.05.105

Cummings, J., & Smedstad, O.-M. (2013). Variational data assimilation for the global ocean. In S. K. Park & L. Xu (Eds.), *Data assimilation for atmospheric, oceanic and hydrological applications* (Vol. 2, pp. 303–343). Berlin: Springer. https://doi.org/10.1007/978-3-642-35088-7

Derber, J., & Rosati, A. (1989). A global oceanic data assimilation system. *Journal of Physical Oceanography*, *19*(9), 1333–1347. https://doi.org/10.1175/1520-0485(1989)019<1333:AGODAS>2.0.CO;2

Di Lorenzo, E., Moore, A. M., Arango, H. G., Cornuelle, B. D., Miller, A. J., Powell, B. S., et al. (2007). Weak and strong constraint data assimilation in the Inverse Ocean Modelling System (ROMS): Development and application for a baroclinic coastal upwelling system. *Ocean Modelling*, *16*(3-4), 160–187. https://doi.org/10.1016/j.ocemod.2006.08.002

Egbert, G. D., Bennett, A. F., & Foreman, M. G. (1994). Topex/Poseidon tides estimated using a global inverse model. *Journal of Geophysical Research*, *99*(C12), 24,821–24,852. https://doi.org/10.1029/94JC01894

Fenty, I., & Heimbach, P. (2013). Coupled sea ice-ocean-state estimation in the Labrador Sea and Baffin Bay. *Journal of Physical Oceanography*, *43*(5), 884–904. https://doi.org/10.1175/JPO-D-12-065.1

Hebert, D. A., Allard, R. A., Metzger, E. J., Posey, P. G., Preller, R. H., Wallcraft, A. J., et al. (2015). Short-term sea ice forecasting: An assessment of ice concentration and ice drift forecasts using US Navy's Arctic Cap Nowcast/Forecast System. *Journal of Geophysical Research: Ocean*, *120*(12), 8327–8345. https://doi.org/10.1002/2015JC011283

Helfrich, S. R., McNamara, D., Ramsay, B. H., Baldwin, T., & Kasheta, T. (2007). Enhancements to, and forthcoming developments in the Interactive Multisensor Snow and Ice Mapping System (IMS). *Hydrological Processes*, *21*(12), 1576–1586. https://doi.org/10.1002/hyp.6720

Hogan, T. F., Liu, M., Ridout, J. A., Peng, M. S., Whitcomb, T. R., Ruston, B. C., et al. (2014). The Navy Global Environmental Model. *Oceanography*, *27*(3), 116–125. https://doi.org/10.5670/oceanog.2014.73

Hunke, E.C., Lipscomb, W.H., Turner, A.K., Jeffery, N., & Elliott, S., (2015). CICE: The Los Alamos Sea Ice Model, Documentation and Software User's Manual, version 5.1. Tech. Rep. LA-CC-06-012. Los Alamos, New Mexico: Los Alamos National Laboratory. Retrieved from http://oceans11.lanl.gov/trac/CICE\#no1

King, J., Skourup, H., Hvidegaard, S. M., Rösel, A., Gerland, S., Spreen, G., et al. (2018). Comparison of freeboard retrieval and ICE thickness calculation from ALS, ASIRAS, and CryoSat-2 in the Norwegian Arctic, to field measurements made during the N-ICE2015 expedition. *Journal of Geophysical Research: Ocean*, *123*(2), 1123–1141. https://doi.org/10.1002/2017JC013233

Koldunov, N., Köhl, A., Nuno Serra, N., & Stammer, D. (2017). Sea Ice Assimilation into a coupled ocean-sea ice adjoint model of the Arctic Ocean. *The Cryosphere*. https://doi.org/10.5194/tc-2017-2

Koldunov, N. V., Köhl, A., & Stammer, D. (2013). Properties of adjoint sea ice sensitivities to atmospheric forcing and implications for the causes of the long term trend of Arctic sea ice. *Climate Dynamics*, *41*(2), 227–241. https://doi.org/10.1007/s00382-013-1816-7

Krishfield, R. A., Proshutinsky, A., Tateyama, K., Williams, W. J., Carmack, E. C., McLaughlin, F. A., & Timmermans, M.-L. (2014). Deterioration of perennial sea ice in the Beaufort Gyre from 2003 to 2012 and its impact on the oceanic freshwater cycle. *Journal of Geophysical Research: Oceans*, *119*, 1271–1305. https://doi.org/10.1002/2013JC008999

Kwok, R., Cunningham, G. F., Wensnahan, M., Rigor, I., Zwally, H. J., & Yi, D. (2009). Thinning and volume loss of the Arctic Ocean sea ice cover: 2003–2008. *Journal of Geophysical Research*, *114*, C07005. https://doi.org/10.1029/2009JC005312

Laxon, S. W., Giles, K. A., Ridout, A. L., Wingham, D. J., Wilatt, R., Cullen, R., et al. (2013). CryoSat-2 estimates of Arctic sea ice thickness and volume. *Geophysical Research Letters*, *40*, 732–737. https://doi.org/10.1002/grl.50193

Lindsay, R. W., & Zhang, J. (2006). Assimilation of ice concentration in an ice-ocean model. *Journal of Atmospheric and Oceanic Technology*, *23*(5), 742–749. https://doi.org/10.1175/JTECH1871.1

Lisäter, K. A., Evensen, G., & Laxon, S. (2007). Assimilating synthetic CryoSat-2 sea ice thickness in a coupled ice–ocean model. *Journal of Geophysical Research*, *112*, C07023. https://doi.org/10.1029/2006JC003786

Lisäter, K. A., Rosanova, J., & Evensen, G. (2003). Assimilation of ice concentration in a coupled ice–ocean model, using the ensemble Kalman filter. *Ocean Dynamics*, *53*(4), 368–388. https://doi.org/10.1007/s10236-003-0049-4

Metzger, E. J., Posey, P. G., Thoppil, P. G., Townsend, T. L., & Wallcraft, A. J. (2015). Validation test report for the Global Ocean Forecast System V3.1–1/12° HYCOM/NCODA/CICE/ISOP. NRL Memo. Report NRL/MR/7320--15-9579.

Mu, L., Yang, Q., Losch, M., Losa, S. N., Ricker, R., Nerger, L., & Liang, X. (2018). Improving sea ice thickness estimates by assimilating CryoSat-2 and SMOS sea ice thickness data simultaneously. *Quarterly Journal Of The Royal Meteorological Society*, *144*, 529–538.

Proshutinsky, A., Krishfield, R., Timmermans, M.-L., Toole, J., Carmack, E., McLaughlin, F., Williams, W. J., et al. (2009). The Beaufort Gyre freshwater reservoir: State and variability from observations. *Journal of Geophysical Research*, *114*, C00A10. https://doi.org/10.1029/2008JC005104

Ricker, R., Hendricks, S., Helm, V., Skourup, H., & Davidson, M. (2014). Sensitivity of CryoSat-2 Arctic sea ice freeboard and thickness on radar-waveform interpretation. *The Cryosphere*, *8*, 1607–1622.

Serreze, M. C., & Stroeve, J. (2015). Arctic sea ice trends, variability and implications for seasonal ice forecasting. *Philos. Trans. R. Soc. A*, *373*, 1–16. https://doi.org/10.1098/rsta.2014.0159

Shlyaeva, A., Buehner, M., Caya, A., Lemeieux, J.-F., Smith, G. C., Roy, F., et al. (2016). Towards ensemble data assimilation for the Environment Canada Regional Ice Prediction System. *Quarterly Journal of the Royal Meteorological Society*, *142*, 1090–1099.

Stark, J. D., Ridley, J., Martin, M., & Hines, A. (2008). Sea ice concentration and motion assimilation in a sea ice ocean model. *Journal of Geophysical Research*, *113*, C05S91. https://doi.org/10.1029/2007JC004224

Tateyama, K., Krishfield, R. A., Williams, W. J., & Enomoto, H. (2013). Estimation of Arctic sea ice thickness from satellite passive microwave radiometers. *3rd International Symposium on the Arctic Research* (ISAR-3), Tokyo, Japan, 14–17 January. Retrieved from http://www.jcar.org/isar-3/abstracts/S6_oral.pdf

Tian-Kunze, X., Kalescke, L., Maass, N., Makynen, M., Serra, N., Drusch, M., & Krumpen, T. (2014). SMOS-derived sea ice thickness: Algorithm baseline, product specifications and initial verification. *The Cryosphere*, *8*, 643–646.

Tietsche, S., Notz, D., Jungclaus, J. H., & Marotzke, J. (2013). Assimilation of sea-ice concentration in a global climate model—Physical and statistical aspects. *Ocean Science*, *9*, 19–36. https://doi.org/10.5194/os-9-19-2013

Wang, K., Debernard, J., Sperrevik, A. K., Isachsen, P. E., & Lavergne, T. (2013). A combined optimal interpolation and nudging scheme to assimilate OSISAF sea-ice concentration into ROMS. *Annals of Glaciology*, *54*(62). https://doi.org/10.3189/2013AoG62A138

Warren, S. G., Rigor, I. G., Untersteiner, R., Radionov, V. F., Bryazgin, N. N., Aleksandrov, Y. I., & Colony, R. (1999). Snow depth on Arctic Sea ice. *Journal of Climate*, *12*, 1814–1829.

Weaver, A. T., & Courtier, P. (2001). Correlation modeling on a sphere using a generalized diffusion equation. *Quarterly Journal of the Royal Meteorological Society*, *127*, 1815–1846.

Weaver, A. T., & Mirouze, I. (2013). On the diffusion equation and its application to isotropic and anisotropic correlation modeling in variational assimilation. *Quarterly Journal of the Royal Meteorological Society*, *139*, 242–260.

Weaver, A. T., Tshimanga, J., & Piacentini, A. (2015). Correlation operators based on an implicitly formulated diffusion equation solved with Chebyshev iteration. *Quarterly Journal of the Royal Meteorological Society*, *142*, 455–471. https://doi.org/10.1002/qj.2664

Weaver, A. T., Vialard, J., & Anderson, D. L. T. (2003). Three- and four-dimensional variational assimilation with a general circulation model of the Tropical Pacific Ocean. Part I: Formulation, internal diagnostics and consistency checks. *Monthly Weather Review*, *131*, 1360–1378.

Yang, Q., Losa, S. N., Losch, M., Liu, J., Zhang, Z., Nerger, L., & Yang, H. (2015). Assimilating summer sea-ice concentration into a coupled ice-ocean model using a LSEIK filter. *Annals of Glaciology*, *56*(69), 38–44.

Yang, Q., Losa, S. N., Losch, M., Tian-Kunze, X., Nerger, L., Lui, J., et al. (2014). Assimilating SMOS sea ice thickness into a coupled ice-ocean model using a local SEIK filter. *Journal of Geophysical Research: Oceans*, *119*, 6680–6692. https://doi.org/10.1002/2014JC009963

Yang, Q., Losch, M., Losa, S. N., Jung, T., & Nerger, L. (2016). Taking into account atmospheric uncertainty improves sequential assimilation of SMOS sea ice thickness data in an ice-ocean model. *Journal of Atmospheric and Oceanic Technology*, *35*, 397–407.

Yaremchuk, M., & Carrier, M. (2012). On the renormalization of the covariance operators. *Monthly Weather Review*, *140*(2), 637–649.

Yaremchuk, M., Carrier, M., Smith, S., & Jacobs, G. (2013). Background error correlation modeling with diffusion operators. In S. K. Park & L. Xu (Eds.), *Data assimilation for atmospheric, oceanic and hydrological applications* (Vol. 2, pp. 177–203). Berlin: Springer. https://doi.org/10.1007/978--3-642-35088-7_8

Yaremchuk, M., & Nechaev, D. (2013). Covariance localization with the diffusion-based correlation models. *Monthly Weather Review*, *141*(2), 848–860.

Yaremchuk, M., & Smith, S. (2011). On the correlation functions associated with polynomials of the diffusion operator. *Quarterly Journal of the Royal Meteorological Society*, *137*, 1927–1932.